The Cryosphere Discuss., 6, 2961–3010, 2012
www.the-cryosphere-discuss.net/6/2961/2012/
doi:10.5194/tcd-6-2961-2012

The Cryosphere Discussions

Effect of higher-order stress gradients on the centennial mass evolution of the Greenland ice sheet

J. J. Fürst, H. Goelzer, and P. Huybrechts

Vrije Universiteit Brussel, Earth System Sciences and Departement Geografie, Pleinlaan 2, Brussel, Belgium

Received: 26 June 2012 – Accepted: 10 July 2012 – Published: 27 July 2012

Correspondence to: J. J. Fürst (johannes.fuerst@vub.ac.be), H. Goelzer (heiko.goelzer@vub.ac.be), and P. Huybrechts (philippe.huybrechts@vub.ac.be)

Published by Copernicus Publications on behalf of the European Geosciences Union.

Abstract

We use a three-dimensional thermo-mechanically coupled model of the Greenland ice sheet to assess the effects of marginal perturbations on volume changes on centennial time scales. The model is designed to allow for five ice dynamic formulations using different approximations to the force balance. The standard model is based on the shallow ice approximation for both ice deformation and basal sliding. A second model version relies on a higher-order Blatter/Pattyn type of core that resolves effects from gradients in longitudinal stresses and transverse horizontal shearing, i.e. membrane-like stresses. Together with three intermediate model versions, these five versions allow for gradually more dynamic feedbacks from membrane stresses. Idealised experiments were conducted on various resolutions to compare the time-dependent response to imposed accelerations at the marine ice front. If such marginal accelerations are to have an appreciable effect on total mass loss on a century time scale, a fast mechanism to transmit such perturbations inland is required. While the forcing is independent of the model version, inclusion of direct horizontal coupling allows the initial speedup to reach several tens of kilometres inland. Within one century, effects from gradients in membrane stress alter the inland signal propagation and transmit additional dynamic thinning to the ice sheet interior. But the centennial overall volume loss differs only by some percents from the standard model as the dominant response is a diffusive inland propagation of geometric changes. In our experiments, the volume response is even attenuated by direct horizontal coupling. The reason is a faster adjustment of the sliding regime by instant stress transmission in models that account for the effect of membrane stresses. Ultimately, horizontal coupling decreases the reaction time to perturbations at the ice sheet margin.

TCD
6, 2961–3010, 2012

1 Introduction

The Greenland ice sheet (GrIS) is a highly dynamic system where net accumulation is compensated by both surface ablation and dynamic discharge at the marine margin. The system is closed by ice motion and it was essentially in balance in the decade preceding this millennium (Zwally et al., 2005; van den Broeke et al., 2009; Rignot et al., 2011). For the present state, this mass turn-over is stated to be out of balance and recent estimates for current mass loss rates based on gravimetry (Luthke et al., 2006; Velicogna et al., 2009; Schrama and Wouters, 2011), on radar/laser altimetry (Slobbe et al., 2008; Sørensen et al., 2011; Zwally et al., 2011; Moon et al., 2012) and on approaches combining radar discharge estimates with surface mass balance modelling (van den Broeke et al., 2009; Rignot et al., 2011) range from 0.3–0.8 mm s.l.e. yr^{-1} (110–290 Gt yr^{-1}). About two-thirds of this accelerated mass loss are attributed to increased runoff, while observed outlet glacier speed-up export the other third (Rignot and Kanagaratnam, 2006; Rignot et al., 2011). Although outlet glacier retreat is observed all around Greenland, its onset is described either by synchronous speed-up (Thomas et al., 2009), or at least by regionally linked accelerations (Howat et al., 2008; Howat and Eddy, 2011), or by more erratic behaviour for other regions (Howat et al., 2010; Joughin et al., 2010; McFadden et al., 2011, Moon et al., 2012). In other words, observations provide only mere indications for possible reasons of such accelerations. Hypotheses range from enhanced basal lubrication by increased summer melt (Zwally et al., 2002; Joughin et al., 2008; Bartholomew et al., 2010; Sundal et al., 2011; Schoof, 2010), to cryo-hydrologic warming by melt drainage (Phillips et al., 2010), ocean-induced grounding line retreat (Schoof, 2007; Briner et al., 2009) or enhanced calving activity (Benn et al., 2007; Nick et al., 2010). Loss of buttressing at the glacier front is believed to be induced either by local surface melt (Scambos et al., 2000), hydro-fracturing and subsequent front destabilisation or by intrusion of warm, saline ocean water into the local fjord systems triggering submarine melting (Holland et al., 2008; Amundson et al., 2010; Straneo et al., 2010, 2011; Motyka et al.,

TCD
6, 2961–3010, 2012

2011; Christofferson et al., 2011). Except for cyclic surge behaviour, observations indicate that accelerations are mostly triggered in the marine-terminated ablation area. This area constitutes a small fraction of the entire GrIS extent and instant effects from speed-up remain confined to the periphery. Such marginal perturbations are directly and indirectly transmitted inland by ice dynamics and the efficiency of this signal transmission controls the impact on the interior (Nick et al., 2009).

One indirect mechanism for signal transmission is diffusive surface elevation adjustment. Marginal perturbations alter the local ice thickness and surface slope, which in turn affects the flow in its close vicinity. The surrounding geometry consequently adjusts and thereby the signal is gradually transmitted inland. The efficiency of this indirect signal transmission is controlled by ice viscosity, which readily covers several orders of magnitude. The effects of diffusive geometry adjustment are well understood and have been studied in models for large-scale ice sheets both on long and short time-scales (Huybrechts and de Wolde, 1999; Ritz et al., 2001). However, there are also direct mechanisms that can instantaneously transmit marginal perturbations inland. One potential candidate for direct signal transmission is inherent in the local force balance within a solid body of ice. Horizontal gradients either in pure shear or simple shear are capable of instantaneously transmitting signals to the close vicinity (Kamb and Echelmeyer, 1986). In particular gradients in membrane-like stresses (see Hindmarsh, 2006) are suspected of efficient horizontal coupling. These stresses are often referred to as "longitudinal stresses" owing to an extensive study of plane flow setups. In this paper, longitudinal stresses will strictly be distinguished from transverse horizontal shearing as the two representatives of membrane-like stresses.

From a theoretical point, longitudinal coupling in an ice sheet is efficient within a domain of four to ten times the ice thickness (Kamb and Echelmeyer, 1986). This coupling length increases with the non-linear character of the viscous material and we therefore expect values of 5–40 km on the GrIS. For a plane flow setup on Jakobshavn Isbræ, Price et al. (2008) succeeded to explain instant accelerations observed at Swiss Camp by longitudinal transmission of near margin perturbations. With a linear flow and sliding

TCD
6, 2961–3010, 2012

law, they solve the full force balance equation and estimate that horizontal coupling has a 10–15 km area of direct influence. For a similar plane flow application on Helheim, Nick et al. (2009) highlight the transient propagation of perturbations initiated at the glacier terminus. The immediate response confirms a 10 km coupling radius to the applied marginal forcing. Accounting for pseudo-plasticity of ice and for non-linear sliding, the effective longitudinal coupling length is expected to increase while for typical Antarctic ice streams it shows values of about 40 km (Williams et al., 2012). Such plane flow setups are however limited to the effect of longitudinal stress gradients and omit effects from transverse shearing which widely occur in many stream-like outlet glaciers embedded in the GrIS. Moreover, the purpose of such flow line setups is often to reproduce observed flow evolution rather than the study of the influence of direct horizontal coupling on the geometry evolution.

In this paper, we apply a 3-D thermo-mechanically coupled Greenland ice flow model that includes the option to activate direct stress transmission via gradients in longitudinal stresses and in transverse horizontal shearing. At first, the model is described in Sect. 2 together with a justification for its applicability to direct stress transmission. Section 3 sets the experimental frame for the centennial perturbation scenarios on Greenland while results are subsequently discussed in Sect. 4. Introduction of an instant reaction time scale provides a tool to summarise results from all experiments for different resolutions and model versions in Sect. 5. Before the final conclusion, a discussion of the entire model setup assesses the reliability of the results.

2 Model description and terminology

2.1 Stress terminology

The fundamental force balance is presented in Appendix A and serves as basis for our stress terminology. Based on scaling arguments, vertical plane shearing (σ_{xz}, σ_{yz}) exerts major control on the dynamics of large-scale grounded ice bodies, as exemplified

TCD
6, 2961–3010, 2012

in the shallow ice approximation (SIA; Hutter et al., 1983). Following the terminology in Hindmarsh (2006), normal stresses acting in horizontal direction (σ_{xx}, σ_{yy}) and horizontal shearing on vertical planes (σ_{xy}, σ_{yx}) are referred to as membrane-like or simply membrane stresses. Here we refer to σ_{xx}, σ_{yy} as the longitudinal stresses acting in the horizontal direction parallel to the normal vector of the respectively addressed surface. The other two membrane stresses we refer to as transverse horizontal shear stresses (σ_{xy}, σ_{yx}), or simply transverse horizontal shearing. Dynamics arising from gradients in longitudinal stresses or transverse horizontal shearing are addressed as effects of membrane stress gradients, direct horizontal stress/signal transmission or direct horizontal coupling. The remaining three components of the stress tensor are the normal stress in the vertical σ_{zz} and vertical plane shearing σ_{zx}, σ_{zy}. This terminology is linked to the imposed coordinate system and best applicable to large-scale and simple geometries. For generalisation to more complex geometries a consistent and precise terminology will depend on local geometry.

2.2 General model characteristics

The three-dimensional, thermo-mechanically coupled ice sheet model comprises three main components that respectively describe the ice rheology, the Earth crust's isostatic rebound and the mass balance at the upper and lower ice sheet boundaries (Huybrechts and de Wolde, 1999; Huybrechts, 2002; to which the interested reader is referred for a detailed description of all model components). The optional higher-order (HO) ice-dynamic core is described in Fürst et al. (2011). Ice dynamics, isostatic adjustment and mass balance are implemented on a computational grid with 5 km horizontal resolution and 30 non-equidistant layers. The vertical grid spacing is refined towards the bottom where vertical plane shearing is concentrated. Geometric input has been modified from the original Bamber et al. (2001) data as described in Huybrechts et al. (2011).

TCD
6, 2961–3010, 2012

2.3 Model versions for ice dynamics

The ice-dynamic model component is based on a viscous rheology assuming isotropy within the ice body. Ice flow results from internal deformation together with sliding over soft till or bedrock but is limited to areas where basal temperatures are within 1 °C of the pressure melting point. Modelled ice creep follows a Glen-type constitutive relation (Eq. A3) that links the stress field to strain rates in analogy to a viscous material with an exponent of three. The proportionality factor also depends on ice temperature and ice age. Together with the force balance (Eq. A1) and incompressibility equation (Eq. A2) they form the most general set of equations for ice deformation, solved for in so-called Full-Stokes (FS) models (Zwinger et al., 2007; Jouvet et al., 2009; Seddik et al., 2012). In our approach, this system of equations is not solved in its full complexity but different approximations are applied concerning ice deformation and basal resistance. This results in altogether five different model versions (cf. Table 2 and refer to Appendix A and B for details).

For ice deformation our model optionally applies the classical SIA approach or a LMLa higher-order core (Fürst et al., 2011). The latter version captures dynamic feedbacks arising from gradients in membrane stresses (see Sect. 2.1). These two options are combined with either of three possible descriptions of basal resistance. A first approach assumes that basal resistance locally supports all of the driving stress (DR). A second approach uses the shallow shelf approximation as a sliding law (ME) (cf. Schoof and Hindmarsh, 2009; Bueler and Brown, 2009). In this case, resistance at the base is dominated by membrane stresses while any effect from vertical shearing on sliding is neglected. Reconciling these two extremes approaches, a simplified resistance (SR) equation includes effects from both vertical plane shearing and membrane stresses at the base. The simplification used in this third approach is inherited from the HO ice deformation and stems from a scale analysis of gradients in the velocity field (see Appendix B).

TCD
6, 2961–3010, 2012

Table 2 summarizes the six model versions combining ice creep and basal resistance. DR SIA corresponds to the shallow ice approximation where basal resistance equals the driving stress. In this setup the solution is purely local and in situ geometry dictates the velocity field. Consequently there is no direct signal transmission between neighbouring ice columns and communication is restricted to diffusive propagation. Another approach to allow for direct horizontal stress transmission is to limit it to the basal layer via sliding but to keep the local SIA formulation within the overlying ice body. Recent approaches use the shallow shelf approximation to describe basal resistance (Ritz et al., 2001; Bueler and Brown, 2009) neglecting vertical plane shearing at the base. In our ME SIA setup, membrane stresses take full control on basal velocities but horizontal signal transmission is restricted to areas that indeed slide. A similar approach reconciles influences from both membrane stresses and vertical plane shearing yet a minor simplification is applied in the basal balance of resistive stresses (SR). Note that the SR SIA version actually needs a full determination of the 3-D higher-order solution in order to extract the velocity field at the base. The switch to a HO approach for ice deformation allows horizontal coupling beyond areas of sliding. Combining such deformation with a geometrically prescribed basal resistance gives the DR HO setup. Including direct signal transmission in the basal layer, one either opts for a pure membrane stress ME HO variant or the fully coupled higher-order model with the simplified resistance at the base SR HO. Both would allow for signal transmission feedbacks between basal dynamics and creep in the ice body above. However, since the latter version is more self-consistent and natural, the ME HO setup is not considered in our assessment of the GrIS' dynamic response.

3 Experimental design

The experimental frame for this study is set by three schematic perturbation scenarios and focuses on the centennial response of the GrIS. The aim is to investigate effects of direct horizontal coupling on the projected volume evolution. These experiments serve

TCD
6, 2961–3010, 2012

both as an intercomparison study for the five model versions with different dynamic complexity and as an assessment of the range of dynamic ice loss in the future. Optional grid spacing of 20, 10 or 5 km allows us to investigate the impact of resolution on capturing direct signal transmission.

3.1 Initialisation

As standard initial conditions serves an interglacial equilibrium. The climatic forcing is obtained from a generic temperature field that depends on latitude and surface elevation (details in Huybrechts, 2002). The initialisation on 5 km takes 25 kyr and is preceded by a 200 and a 100 kyr equilibrium run on respectively 20 and 10 km. For this spin-up the DR SIA model setup is chosen and we denote this standard interglacial with "IS". For assessing the robustness of the results under different initial conditions, we experimented with two other spin-up methods. The first one uses the SR HO model version to produce the interglacial equilibrium. It starts from the respective IS geometry and is evolved for either 50, 20 and 5 kyr to an initial state "IH". For the second initialisation method, the model is spun up over the last two glacial cycles in the same way as described in Huybrechts et al. (2011). The resolution was successively increased from 20 km to 10 km at 20 kyr BP and to 5 km at 3 kyr BP. However the general outcome did not depend much on the specific initialisation technique and in the following we present results based on the IS spin-up.

3.2 Perturbation experiments

We conduct three types of experiments that address various aspects of Greenland's ice dynamic response (cf. Table 3). Their focus is on the century timescale while they are designed in a way that each model version is applicable. The central experiment prescribes a step function in the basal sliding coefficient A_{sl} but spatially confines this amplification to the marine terminated boundary (experiment MarAsl2). Our choice for an A_{sl} amplification factor of 2 with a spatial extent of 40 km upstream of the marine

TCD
6, 2961–3010, 2012

boundary is loosely based on the details of the 1992/2002 speed-up of Jakobshavn Isbræ (Joughin et al., 2008). This experiment allows us not only to analyse differences in dynamic discharge but also to investigate the actual signal transmission towards the ice sheet interior. In a second experiment (TotAsl2), the basal sliding coefficient is also doubled but now over the entire sliding area. This experiment can be considered as an extreme lubrication event, which by far exceeds the ablation area. In a last experiment, the model response to a massive singular ice removal event at the marine margin around Greenland is investigated. Grid cells that have a marine boundary are instantaneously emptied. In order to ensure comparability between all resolutions ice removal is enforced up to 20 km inland.

To enable a clean comparison between the five model versions, we determine ice velocities in the first grounded point based on the DR SIA model version. This provides unified perturbations for all experiments. Otherwise we would introduce numerical differences in the implementation of the lateral boundary conditions originating from the non-local influence on the velocity solution in model versions with horizontal coupling, which requires zero velocity outside the ice sheet. Although this approach inhibits membrane stress activity in the first grounded ice point, none of the used resolutions actually resolve the full dynamic complexity in theses zones. This choice also confines feedbacks from the five dynamic models to the inland transmission. Additional tests (not shown) brought to light that applying DR SIA at the first grounded point either all around Greenland or restricted to the marine margin has no significant influence on the presented results. Unperturbed control runs are conducted to assess the effects of model adjustment and background evolution.

4 Results

In the IS initialisation, the geometry is in equilibrium with the internal DR SIA equations. The ice sheet extent and volume for this IS geometry are close to the present day configuration (cf. Fig. 1), though such a geometric agreement is not crucial to stress

TCD
6, 2961–3010, 2012

differences in ice-dynamic response amongst our model versions. A notable mismatch is the excess of ice on Pearyland arising from shortcomings in bed topography and surface mass balance. The associated velocity field on this 5 km resolution resolves several narrow stream features that appear at locations where recent observations show equivalent fast ice flow (cf. Fig. 1 and Joughin et al., 2010). Prominent examples are Jakobshavn Isbræ in the west, Helheim Glacier and Kangerlugssuaq in the east, and Nioghalvfjerdsbræ, Zachariæ Isstrøm and Petermann Isstrøm in the north. Together these glaciers drain about 33 % of the total calving flux from the GrIS (Rignot and Kanagarathnam, 2006). This equilibrium velocity field however fails to generate one prominent detail, the long Northeast Greenland Ice Stream feeding Zachariae Isstrøm and Storstrømmen. This is partly explained by insufficient knowledge of the bed topography in this region and may be linked to an additional source of geothermal heat from subglacial volcanos (Buchardt and Dahl-Jensen, 2007). The 5 km velocity field captures flow features which do not appear on a 20 km grid. Such details arise naturally from resolved details in bedrock topography and basal heating. They are not the result from optimising the basal sliding coefficient to match the observed velocity field as in Price et al. (2011).

In our setup, the IS surface velocity field is in equilibrium with the DR SIA equations and the continuity equation. This enables a comparison with the SR HO variant computed diagnostically (Fig. 1). The two velocity fields largely resemble each other and the effect of higher-order dynamics becomes only apparent in some details (Fig. 1c, d). The DR SIA velocity magnitude exhibits sharper features that are effectively smoothed by direct horizontal coupling in the full higher-order version. This first evidence for membrane stress gradients is confirmed by the fact that near the ice divide velocities tend to be higher in the SR HO version. This can be explained by velocity gradients that become important for ice deformation in the absence of pronounced surface slopes and driving stresses close to the ice divides. But also effects from transverse horizontal shear are readily visible across narrow ice streams where fast stream velocities couple with the stagnant surroundings (see e.g. Kangerlugssuaq Fig. 1c, d).

TCD
6, 2961–3010, 2012

In the following the transient effect of direct horizontal coupling is studied on various resolutions. First the GrIS volume evolution is determined for our perturbation experiments (cf. Table 3). The GrIS mass loss for MarAsl2 is then decomposed in a pure dynamic signal and a component arising from the feedback with surface mass balance. The dominant dynamic feedback is further investigated by comparing all model versions. To better analyse results covering all model versions, grid resolutions and marginal perturbation experiments, we finally introduce a reaction timescale to characterise their individual response behaviour.

4.1 Dynamic discharge

For all experiments, the total volume loss of the GrIS after one century falls into a range of 1 and 12 cm of equivalent eustatic sea-level change (s.l.e.), cf. Fig. 2. All of the suggested perturbation experiments are very schematic as a simultaneous outlet speed-up is enforced. For such quite extreme scenarios, the modelled range of mass loss of some centimetres within one century can in fact be considered small. But such magnitudes are fully in line with estimates for present-day rates of increased dynamic ice export of about 0.2–0.4 mm s.l.e. yr^{-1} (van den Broeke et al., 2009) and projections for the dynamic response (Price et al., 2011). The results have to be interpreted in terms of Greenland's total mass balance. The modelled net accumulation for our IS equilibrium is equivalent to 1.5 mm s.l.e. yr^{-1}. It is balanced by surface runoff and ice discharge at rates of 0.84 (55 %) and 0.66 mm s.l.e. yr^{-1} (45 %), respectively. Doubling of ice discharge would therefore extrapolate to a mass loss of about 66 mm s.l.e. within hundred years in case this rate can be sustained. However, all experiments show that initial mass loss rates are not sustained and are in fact damped by dynamic feedbacks. For a doubling of sliding over the entire sliding area (TotAsl2), discharge rates can not be maintained. They gradually decrease and add up to a mass loss of 40 mm s.l.e. after one century (Fig. 2c). For the marginal perturbation in MarAsl2 (Fig. 2a), mass loss rates are even faster attenuated due to a lack of upstream inflow, generating about 16 mm of centennial sea level contribution. In a similar way, the initial release of some

TCD
6, 2961–3010, 2012

40 mm s.l.e. ice volume in the MarCut experiment is succeeded by a quick decrease in mass loss rates (Fig. 2d), which in one century integrates to 85 mm s.l.e. Rerunning the MarAsl2 experiment from the IH interglacial or from the present PS state (cf. Fig. 2b) qualitatively shows the same cumulative mass loss. The MarAsl2 experiment was also repeated with amplification factors of five and ten, showing that the centennial mass loss scales almost linearly for such forcing magnitudes (not shown).

A comparison of the different model versions shows that their response magnitudes are very similar (see Fig. 2). Differences lie within 20 % of the total signal, so effects from the ice-dynamic complexity of each model version are relatively small. Notably for experiments where the sliding parameter was amplified (Fig. 2a, c), an increase in dynamic complexity actually reduces the centennial mass loss. This negative feedback is especially strong when activating a full non-linear sliding law (dashed lines in Fig. 2a) reaching 20 % of the total signal. Also for MarCut and TotAsl2, increasing the dynamic complexity reduces the centennial mass loss. Overall, all model versions produce similar results as in the DR SIA setup, where signal transmission is limited by diffusive thinning. The influence of membrane stress gradients on the total mass loss is of secondary importance on all three resolutions (see Sect. 4.4) and is also robust under the various initial states IS, PS and IH.

The fact that the centennial mass loss is dampened as the ice dynamic complexity increases, raises the question whether this is caused by ice dynamics alone or if there is a dominant feedback with surface mass balance. Differences in ice dynamics affect the ice thickness response and together with the elevation feedback change surface runoff (Huybrechts et al., 2002). The MarAsl2 experiment illustrates however that this feedback explains at most 10 % of the mass loss differences between our model versions (see Figs. 2a, 3). For MarAsl2, the magnitude and sign of this feedback is not consistent neither for the various resolutions nor when allowing for direct horizontal coupling. Therefore we exclude it to be the pivotal feedback here. This role is taken by reduced dynamic discharge at the marine ice front which experiences faster attenuation in models including direct horizontal coupling.

TCD
6, 2961–3010, 2012

4.2 Inland propagation of marginal perturbations

For MarAsl2, the reduction in mass loss with dynamic complexity is caused by its impact on the dynamic discharge, i.e. ice calved off at marine margins. This discharge flux depends on the details of the upstream propagation of the perturbations. A first analysis of the initial velocity response will serve to investigate spatial difference in such inland propagation. We conclude this section with a decomposition of the velocity response into its basal and deformational component.

The basal sliding coefficient A_{sl} is doubled within an area extending from the marine front 40 km upstream into the ice sheet. The initial response of the velocity field is shown in Fig. 4 for the three main model versions. Since all experiments start from the same IS equilibrium, the geometry is initially identical. In the DR SIA setup (Fig. 4a, d, e), accelerations are obviously limited to the actually perturbed grid points, which allows us to delineate the A_{sl} amplification zone. Note that the perturbation is also confined to the actual extent of the sliding area, which becomes visible for the close-ups on Jakobshavn Isbræ (Fig. 4d) and Kangerlugssuaq (Fig. 4e). ME SIA (Fig. 4b, f, g) and SR HO (Fig. 4c, h, i) reveal how the initial perturbation instantaneously radiates some distance inland. Effects from both longitudinal stress coupling and transverse horizontal shearing increase the initial area of influence. Transverse horizontal shearing affects a vicinity of about 5–10 km for both model versions, whereas the coupling length for longitudinal stress gradients seems larger. ME SIA exhibits values of about 20 km while SR HO expands the coupling to more than 40 km (cf. Fig. 4f–i). The discrepancy arises from the confinement of membrane stresses to the basal layer for ME SIA whilst their full vertical variation is respected in SR HO. From theoretical arguments, the longitudinal coupling length for linear rheology and ice sheet geometries is expected to vary between four and ten times the ice thickness (Kamb and Echelmeyer, 1986). For ice thicknesses of about 1 km, this is in broad agreement with our modelled speed-up. Reasons for an increase of the coupling length are a nonlinear ice rheology, high sliding or the elongated, deep bed troughs of Greenland outlet glaciers such as

TCD
6, 2961–3010, 2012

for Kangerlugssuaq (Fig. 4e, g, i). The positive influence of basal sliding on the longitudinal coupling length is also emphasised for the Greenland experiment conducted by Price et al. (2008).

Figure 5 illustrates spatial differences in inland signal transmission with respect to DR SIA (upper panels in Fig. 5). For this reference model, changes in ice thickness around Greenland are a result of diffusive thinning. Thickness changes are triggered at the marine margin and are transmitted up to the divide where elevation changes by some millimetres after one century. The thinning pattern of the DR SIA model also delineates the influence area of the diffusive background process. Since diffusive thinning dominates the transient response in all model versions, their thickness evolutions are given with respect to the DR SIA reference. In the first ten years, diffusive inland propagation enhances inland drainage compensating for increased dynamic discharge at the margin. Locally this can result in peripheral thickening (upper panels Fig. 5). In a latter stage, thinning is predominant while sporadic thickening is observed mostly in the east. Here local effects from special bed geometries of individual outlet glaciers come into play.

Activating effects from membrane stress gradients affects both the spatial pattern and the extent of the thinning pattern. In the initial stage, differences relative to the dominant diffusive thinning show enhanced marginal thinning at the marine terminated periphery. An additional decrease in ice thickness there reduces the ice export by calving and provides one explanation for the decreased mass loss (cf. Fig. 1). Initially, direct horizontal coupling does not alter the signal propagation beyond the area of diffusive thinning significantly. But in a later stage, its integrated effect shows up as a thinning signal in the interior, mostly pronounced for model versions that resolve vertical variations in membrane stresses (DR HO and SR HO). Yet in all models, a prominent thickening pattern emerges in the upper regions of the ablation zone in between the marginal and interior thinning. Apart from a few regions, this constitutes the general impact of membrane stress gradients on the geometry evolution in MarAsl2: extra marginal thinning, intermediate thickening and upstream thinning. Though not

TCD
6, 2961–3010, 2012

decisively altering the mass loss response on centennial time scales, this spatial pattern appears to be a fingerprint of resolving membrane stress gradients. The relative thickening of the upper ablation areas arises from downstream damming by the thinned margin. But also upstream accelerations (see Fig. 6) add to this ice bulge in particular for SR HO and DR HO. Since this relative thickening is situated in the upper ablation region, a positive feedback between surface elevation and mass balance amplifies this phenomenon (also see Huybrechts et al., 2002). After 50 yr of geometry evolution, our model versions branch out significantly and velocity fields also hold information on differences in integrated ice thickness changes (see Fig. 6). Very prominent are the relative deceleration in the region of dynamic thickening and the marginal speed-up. ME SIA restricts the effect from membrane stress gradients to the basal layer and velocity differences are dictated by the basal component. The deformational component hardly exceeds this sliding signal (Fig. 6a, c) and additional thinning further upstream remains negligible. Significant speed-up in the interior is seen for the SR HO model. This acceleration mostly arises from amplified ice deformation rather than increased sliding (see Fig. 6b, d) and is therefore a consequence of resolving horizontal membrane stress gradients in the vertical.

Altogether, the spatial propagation of marginal perturbations confirms that dynamic complexity indeed alters the geometry evolution but this is far outweighed by the dominant background thickness diffusion. A direct, far field signal transmission can not be confirmed even in the case of full non-linear sliding.

4.3 Decomposition of mass loss attenuation

Direct horizontal coupling causes additional thinning along Greenland's marine margins for the MarAsl2 perturbation. Whether this thinning alone is sufficient to explain the observed mass loss differences between model versions remains unclear. For this purpose, we decompose the dynamic discharge into a contribution from ice thinning alone and from acceleration alone. Since dynamic discharge is proportional to the ice thickness H and the velocity magnitude V near the marine terminated margin, the dynamic

TCD
6, 2961–3010, 2012

discharge difference ΔDD between a perturbed and reference experiment becomes.

$$\Delta DD(t) = DD_P(t) - DD_R(t)$$
$$= C \cdot \int_0^t \left(\overline{V_P}(t')\overline{H_P}(t') - \overline{V_R}(t')\overline{H_R}(t') \right) dt' \quad (1)$$
$$= C \cdot \int_0^t \left(\overline{V_R}(t')\Delta\overline{H}(t') + \Delta\overline{V}(t')\overline{H_R}(t') + \Delta\overline{V}(t')\Delta\overline{H}(t') \right) dt'$$

The discharge difference ΔDD is a cumulative quantity that sums up differences between products of a mean ice thickness $\overline{H}$ and a mean velocity $\overline{V}$. The spatial mean is found by covering all the forced ice points while velocities are vertically averaged. The proportionality factor C has the units of a length scale and depends on the chosen grid spacing. The discharge difference between a perturbed and a reference run consequently depends on three components: differences in ice thickness evolution $\Delta\overline{H} = \overline{H_P}(t) - \overline{H_R}(t)$, differences in velocity evolution $\Delta\overline{V}$ and a combination of both. Their respective signs, shown in Fig. 7, confirm an average increase in velocity magnitude ($\Delta\overline{V} > 0$) and thinning along the margin ($\Delta\overline{H} < 0$). In addition, their magnitudes indicate the dominance of velocity differences for the dynamic discharge evolution. This also confirms that marginal accelerations are not balanced by upstream influx of ice, creating flux divergence and thinning. The cumulative effect from differences in ice thickness evolution alone is one order of magnitude lower than the effect from velocity changes. Accounting for membrane stresses in ice dynamics amplifies the marginal thinning (cf. Fig. 7a) and therefore partially explains the negative feedback on the centennial mass loss (cf. Fig. 2). The combined effect from changes in both velocity and ice thickness (cf. Fig. 7c) adds a small and negative contribution to dynamic discharge. Model versions ultimately diverge because of a different velocity evolution (Fig. 7b). But since the marine margin sees DR SIA velocities, this effect actually arises from their

TCD
6, 2961–3010, 2012

nonlinear dependence on local ice thickness and local surface gradient. Thus marginal DR SIA velocities differ between our model versions according to transient differences in ice influx from upstream.

For a further analysis of the MarAsl2 velocity response with focus on upstream supply, we focus on the sliding area of Greenland below the 2000 m topographic contour. The resulting region provides the main supply for dynamic discharge at the marine margin. We additionally decompose the velocity field into its sliding component and the vertically averaged, deformational component (Fig. 8). Both components show an instant increase after the perturbation is activated, which in average is about 250 $\mathrm{m\,yr^{-1}}$ for sliding and 17 $\mathrm{m\,yr^{-1}}$ for deformation. This acceleration is for both components attenuated fast. The deformational component almost completely returns to the reference value while sliding converges to 120 $\mathrm{m\,yr^{-1}}$. Already the difference in magnitude highlights the importance of the sliding component in transmitting the signal inland. For the attenuation of the sliding signal (Fig. 8a), it is striking that all model versions with basal horizontal coupling (ME SIA, SR SIA, SRHO) group and show a more expressed dampening of the initial perturbation. An integration of this sliding perturbation over time would explain most of the model differences seen in the total mass loss (Fig. 2a). It seems only logic that for a perturbation in the sliding coefficient, it is the sliding velocity that controls the response. But also in the MarCut experiment this dominance is confirmed. However this dominance presumably results from our choice of the respective exponents in the sliding law (Eq. B3) and the flow equation (Eq. A3).

Another notable fact is that DR SIA and DR HO follow a similar sliding attenuation. This is not the case for the deformational component (Fig. 8b), where model versions group according to the used deformational approximation. Especially in the first twenty years, the attenuation for SIA deformation exceeds the weaker dampening in HO models. In essence, differences in ice deformation near the margin neither explain the spread in cumulative discharge (Fig. 2a) nor its magnitude. Dampened ice export results from faster attenuation of the sliding signal near the margin when including membrane stress dynamics.

TCD
6, 2961–3010, 2012

4.4 Reaction times

Accounting for dynamic effects of membrane stresses and the resultant non-local horizontal coupling allows a faster attenuation of the initial perturbation. For quantification, we aim to distil differences in transient responses for each model version, each grid resolution and each experiment into one scalar. We introduce a reaction time based on an exponential decay:

$$\Delta\mathrm{DD}(t) = S \cdot \left(1 - \exp\left(-\frac{t}{\tau_\mathrm{R}}\right)\right) \tag{2}$$

The cumulative dynamic discharge ΔDD has a saturation value S with a mean characteristic reaction time τ_R. The retrieved values are averaged over one century. In this way information from the entire mass evolution enters the two parameters. The resultant mean reaction time shows magnitudes of several decades for marginal forcing (see Fig. 9) but it exceeds hundreds of years for the TotAsl2 perturbation experiment. Since the time series only covers a century, TotAsl2 reaction times are an unconfirmed extrapolation to the data while the system remains far from equilibration. Therefore, we focus on the marginal forcing experiments with clear signal attenuation within our centennial scope.

A common characteristic for all marginal perturbation experiments is the reduction of the reaction time when direct horizontal coupling is active in the basal layer (Fig. 9). The reason is the dominance of sliding on the signal attenuation of the centennial mass loss. However, differences due to our seven model versions remain within 10 % of the DR SIA reference. Reaction time differences arising between a linearisation of the effect of membrane stress gradients in the sliding law and their full non-linear impact (empty circles, Fig. 9a) are small but become more expressed with higher resolution. This again supports their linearization in Appendix B. Yet the response behaviour is rather prone to the chosen grid resolution and reaction times vary up to 40 %. For both marginal perturbation experiments, reducing the grid resolution lowers the reaction time. This would be an undesirable effect if it simply arose from pure grid size reduction.

TCD
6, 2961–3010, 2012

For this reason we repeated all experiments by simply supersampling the 20 km bed topography for the spin-up without using the detailed information from a higher resolution. Then the MarAsl2 set of experiments (not shown) has reaction times of about 40 yr and no monotone dependence on grid resolution. Consequently, the reduced reaction time in our experiments arises from additional information in the input data, which interfere with the spin-up and in turn affect the experimental setup. This behaviour is indeed a wanted effect because geometries are complex in reality and will affect the inland transmission by horizontal coupling via membrane stress gradients. The MarCut experiment however shows the grid dependent reduction of the reaction time in both setups. Here this is a relict from an experimental setup disturbed by grid spacing. While MarAsl2 prescribes a constant 40 km extent of the sliding factor increase, the MarCut perturbation has a direct effect only on the first grounded grid point upstream of the calving points. In summary, a consistent picture emerges for all marginal forcing experiments and for each resolution. Ice sheet reaction times are reduced when direct horizontal coupling operates and therefore allow for a faster attenuation of marginal perturbations. Yet on a century time scale, this faster attenuation does not dominate the total mass loss of the GrIS.

5 Discussion

To assess the effect of direct signal transmission or horizontal coupling on the dynamic response of the GrIS over the next century, five model versions of a 3-D ice-dynamic model were used with different dynamic complexity that spans the gap between the SIA and a higher-order LMLa model for ice evolution. Although effects from membrane stress gradients and their vertical variations are captured, its application is limited by two simplifications (Pattyn, 2003). The decisive one is that the glaciostatic approximation neglects any influence of bridging effects in the vertical force balance. In addition, horizontal gradients in the vertical velocity field are assumed to be negligible compared to vertical gradients in horizontal velocities. One might question whether these

TCD
6, 2961–3010, 2012

two assumptions result in a substantial loss in dynamic complexity that might inhibit important feedbacks for the transient ice sheet behaviour. Based on a scaling from an asymptotic analysis, Schoof and Hindmarsh (2011) present arguments that affirm the applicability of a LMLa model for large aspect ratios. The horizontal component of the LMLa velocity solution shows an error of second order in this ratio. Since the GrIS extent is at least two orders of magnitude larger than its thickness and since the horizontal grid spacing exceeds the thickness, our large-scale ice sheet model remains an appropriate tool for ice dynamics. Although Schoof and Hindmarsh (2011) emphasise the validity of the LMLa approach for slip and non-slip areas separately, the general scaling arguments might be violated in the transition zone (Schoof, 2006). The higher-order LMLa approach is also valid for dynamics in the vicinity of the ice divide where the non-linearity of the viscous material triggers a unique internal layer architecture, the Raymond effect (Raymond, 1983). In general, a LMLa model seems a feasible tool for transient, large-scale applications and it is assumed that additional feedbacks in the FS equations are limited to smaller scales (< 1 km) when stress regimes are well resolved.

Another issue concerns the poorly constrained sliding mechanisms beneath large-scale ice sheets. A recent overview on the controversy concerning sliding theories was presented in Fowler (2010). At the base, a large variety of processes and scales have to be considered and comprised by one theory: bedrock vs. soft till, regelation, bed roughness or characteristic till grain size, water pressure, fracture mechanics (Weertman, 1957, 1964; Lliboutry, 1968; Boulton and Hindmarsh, 1987; Tulaczyk et al., 2000; Schoof, 2005). For basal friction, two prominent approaches are adopted in glaciology, a static Coulomb assumption or a kinematic friction relation. While Coulomb friction enables basal movement above a critical yield stress of the material, the latter links basal resistance directly to local velocities. Our model uses a kinematic approach that is feasible both for soft till and hard bedrock. This Weertman sliding limits sliding to areas where the bed is within 1 °C of the pressure melting point while the third order power law allows for non-linear feedbacks. In fact, the temperature field hardly changes on

TCD
6, 2961–3010, 2012

a centennial time scale, which is equivalent to prescribe the extent of the sliding area. This extent can certainly evolve more dynamically when linking it to basal hydrology. The presence of water beneath the ice sheet pressurises the basal system, balances ice overburden and by lubrication facilitates basal sliding (Zwally et al., 2002). More recent observations (Sundal et al., 2011) and theoretical considerations (Schoof, 2010) however indicate that increased subglacial drainage creates more efficient drainage systems. In such an efficient system, the basal water pressure decreases and so does sliding. This negative feedback naturally limits the effects from basal hydrology on ice dynamics. Nonetheless the basal hydrology and its influence on ice dynamics are central in a realistic description of ice sheet evolution (Bougamont et al., 2011). Another aspect concerns the capability of the sliding relation to transmit perturbation signals. Observations on Rutford Ice Stream (Gudmundsson, 2010) suggest that a non-linear mechanism is a prerequisite to explain the upstream ice response to tidal forcing of different frequencies. Weertman sliding with an exponent of three allows to explain the observed response pattern and seems appropriate to realistically propagate margin signals inland. Altogether, the Weertman sliding, though not allowing for effects from basal hydrology, its formulation in our model allows realistic signal propagation within regions of fast flow. This justifies its use for assessing the influence of direct horizontal coupling on inland signal transmission and the dynamic response of the GrIS.

At a numerical level, our choice of grid spacing remains an optional candidate to alter or potentially inhibit direct horizontal coupling. Since we did not find a strong grid dependence it remains possible that direct horizontal coupling is not resolved properly on all resolutions. First of all, even a 5 km resolution misses small scale features in bed topography such as many narrow bed troughs upstream of outlet glaciers, singular mountain peaks or ridges around Greenland. This deficiency feeds back on ice dynamics and mainly influences the spatial propagation of the initial perturbation signal. In our experiments, reaction times decrease under grid refinement but the overall mass loss response is robust under the three grid choices. For large-scale applications, the integrated influence of dynamic complexity on mass loss is also consistent under

TCD
6, 2961–3010, 2012

resolution changes. Even the initial speed-up (Fig. 4) is in agreement with theoretical estimates for the spatial scale of direct longitudinal coupling (Kamb and Echelmeyer, 1986), which for the GrIS is about 10–20 km. We are therefore convinced that membrane stress activity is captured in an acceptable way in our ice flow model. Except for resolving successively more geometric details, we do not expect that further grid refinement would drastically alter model differences in the spatially integrated mass loss. Underlining the consistency of our results, all of them are robust under different initial conditions (Fig. 2b).

A last point concerns the artificial nature of our perturbation experiments. All of them trigger a dynamically dominated response within one century. But the initial perturbations have in each case a rather extreme character. The MarAsl2 experiment mimics a simultaneous speed-up of the marginal zones of all outlet glaciers around the GrIS while observations indicate a more variable behaviour (Moon et al., 2012). In a similar way, the TotAsl2 experiment doubles velocities within the entire sliding areas, as an attempt to simulate enhanced lubrication due to increased surface melt. The spatial extent, the duration and the magnitude of the amplification in TotAsl2 exceed by far the values from recent observations (McFadden et al., 2011; Sundal et al., 2011). Again a simultaneous speed-up is deployed. In MarCut, marginal ice is also removed at the same time and consecutive surface profile thinning is observed. For the three experiments this is the most severe one and the equivalent sea level contribution exceeds 100 mm. Almost half of it is due to the initial ice loss, triggering an additional 80 mm s.l.e. during the following century. The other two experiments result in a centennial sea level contribution of 45 mm and 16 mm. Since the experiments are extreme, as is also the case for the dynamic discharge in Price et al. (2011), these numbers should be considered as upper limits. Gravensen et al. (2010) account for outlet glacier speed-up under future climate scenarios and mass loss does not exceed 17 cm by the end of the 21st century, including uncertainties from climate projections, future scenarios and outlet speed-up. Though only 15 % or 25 mm of total mass loss are associated with outlet accelerations, it implies an immense speed-up around entire Greenland. But their DR

TCD
6, 2961–3010, 2012

SIA ice sheet model also predicts fast attenuation of the initial amplification of sliding velocities by dynamic thinning at the margin. In MarAsl2, our results suggest enhanced marginal thinning by direct horizontal coupling. Though the additional thinning is not sufficient to cause direct retreat, it perturbs the grounding line position which dependent on the bed slope can trigger a self-accelerated retreat (Schoof, 2007). However such retreats are geometrically limited by the bathymetry of the outlet glacier fjords because bed elevation mostly exceeds sea level within several tens of kilometres inland from the present ice front.

6 Conclusion

A thermo-mechanically coupled 3-D large-scale ice sheet model with five versions of dynamic complexity was used to assess the influence of membrane stress gradients on the centennial response of the GrIS under various marginal perturbations. Results indicate that the SIA, which does not include effects from direct horizontal coupling, already captures the major response characteristics. The inclusion of membrane stress gradients in various ways in fact reduces the volume response by 20 % at most from different inland propagation of marginal perturbations. Models that include direct horizontal coupling are capable of attenuating perturbations faster by instant upstream propagation. Additionally, our results exclude that the process that alters cumulative mass loss is an interaction with surface mass balance via surface elevation changes. For MarAsl2, a reduction of dynamic discharge at the marine margin prevents accelerated mass loss. This reduction is not explained by additional marginal thinning alone but by faster attenuation of the initial speed-up, which is caused by a more efficient adjustment of surface slopes. Non-local effects from membrane stresses thus allows for a quicker readjustment to perturbations. The conducted experiments identify sliding as the component that reacts fastest and is capable to explain the differences in mass evolution. Details in the spatially resolved inland propagation of marginal perturbations suggest that model versions, that allow effects from longitudinal stress and transverse

TCD
6, 2961–3010, 2012

horizontal shear gradients, have in each time step a larger area of influence. Yet the general response follows the DR SIA approach for all versions, where signal transmission is accomplished by thickness diffusion alone.

An analysis of all experiments, model versions and grid resolutions reveals that reaction times are primarily dependent on the applied perturbation. The stronger the perturbation and the larger its spatial extent, the longer is the reaction time. Within one experiment, relatively small reductions of reaction time of up to 10 % were found when including direct horizontal coupling. This uniform time scale confirms the negligible effect of the dynamic complexity on the centennial volume evolution of the GrIS.

Our findings have important consequences to decide on the degree of complexity needed when studying the dynamic response to prescribed marginal perturbations. If the interest is in the volume evolution of an ice sheet, the classical SIA approach is sufficient to capture the main characteristics of the inland response. The higher-order approach SR HO is dynamically more complete but the additional computational cost (factor very dependent on chosen accuracies but in our case about 100) is not warranted by the limited gain in ice-sheet volume response. A compromise could be the ME SIA approach (Bueler and Brown, 2009) with direct horizontal coupling in the basal layer. This approach is computationally much more efficient than SR HO (factor 20). Since basal velocity adjustment controls the signal attenuation ME SIA seems more appropriate than DR HO, though computationally they are comparable. Altogether, when SR HO or Full Stokes models become computationally too expensive for a specific setup, we recommend the use of an ME SIA equivalent approach (Hindmarsh, 2006; Bueler and Brown, 2009; Schoof and Hindmarsh, 2009).

Finally, all perturbation experiments performed in this paper had a rather extreme character. Sustained simultaneous speed-up by a factor 2 at all marine margins or in sliding-dominated areas go far beyond observed changes during the last two decades. This strengthens the view that the dominant effect on volume change of the Greenland ice sheet for the 21st century will come from surface mass balance changes. The largest source of uncertainty for future projections of ice sheets therefore arises

TCD
6, 2961–3010, 2012

from the climatic projections used as input rather than from the complexity of the ice-dynamic model.

Appendix A

Variants for ice deformation and basal resistance

A1 Ice deformation

Our glacial system is placed into an orthogonal coordinate system with three unit vectors $\{\boldsymbol{e_x}, \boldsymbol{e_y}, \boldsymbol{e_z}\}$ in respectively horizontal x-, y- and vertical z-direction. The vertical axis of our coordinate system is chosen to be perpendicular to isolines of the gravitational field. In essence ice deformation is based on two balance equations for mass and momentum combined with a constitutive relation that links the stress tensor $\boldsymbol{\sigma}$ to strain rates $\dot{\varepsilon}$ and ultimately to the velocity field $\boldsymbol{u} = (u_x, u_y, u_z)$. Considering an incompressible ice body the balance equations take the following form.

$$\nabla\boldsymbol{\sigma} = -\rho g \boldsymbol{e}_z \tag{A1}$$

$$\nabla\boldsymbol{u} = 0 \tag{A2}$$

Here, the gravitational constant g and the ice density ρ are assumed constant while their respective values are provided in Table 1. Since ice creep is controlled by deviations from cryostatic pressure rather than by the mean pressure itself deviatoric stresses $\tau_{kl} = \sigma_{kl} - \frac{1}{3}\delta_{kl}\sum_m \sigma_{mm}$ (with $k, l, m \in \{x, y, z\}$) are used to link the stress balance to ice deformation. Deviations from the hydrostatic stress give rise to ice deformation. A simple yet reasonably accurate expression relating deviatoric stresses to strain

TCD
6, 2961–3010, 2012

rates for polycrystalline ice is

$$\tau_{kl} = 2\eta\dot{\varepsilon}_{kl} \tag{A3}$$

$$\eta = \frac{1}{2}A(T^{\bullet})^{-\frac{1}{n}}\dot{\varepsilon}_e^{\frac{1-n}{n}} \tag{A4}$$

$$\dot{\varepsilon}_e^2 = \frac{1}{2}\sum_{k,l}\dot{\varepsilon}_{kl}\dot{\varepsilon}_{kl} \qquad \text{with } k,l \in \{x,y,z\} \tag{A5}$$

This constitutive equation is often referred to as Glen's flow law since it was first suggested by John Glen (1955). Here the effective viscosity η serves as proportionality factor while its dependence on the effective strain rate $\dot{\varepsilon}_e$ provides the exponent n for this power law relation. The effective strain rate $\dot{\varepsilon}_e$ in turn is determined as an invariant to the specific coordinate system and it consists of the individual strain components $\dot{\varepsilon}_{kl} = \frac{1}{2}(\partial_l v_k + \partial_k v_l)$. The dependence on pressure melting point corrected temperature $T^{\bullet}$ of the rate factor follows a Arrhenius type function $A(T^{\bullet}) = A_{1/2}\exp(-B_{1/2}/(RT^{\bullet}))$ using two parameters sets for different temperature regimes. The rate factor also shows an age dependence since Wisconsin ice is assumed to deform more readily than Holocene ice for similar stress and temperature conditions. This rheologic influence of the ice age is briefly described in Huybrechts (1994).

Our model offers the possibility to choose between two approximations for solving the Full Stokes (FS) equations (Eqs. A1–A3). Both are simplification of the force balance while the first is the shallow ice approximation (SIA) which is standard practice in modelling large-scale ice sheets. In this approximation any influence from membrane stresses (as defined in Sect. 2.1) is neglected which results in a balance between driving stress and vertical plane shearing.

$$\partial_i \tau_{iz} = -\rho g \partial_i s \qquad \text{with } i,j \in \{x,y\} \tag{A6}$$

Optionally we can determine the stress and velocity field by switching to a higher-order variant (HO) specified as LMLa (Hindmarsh, 2004). In this approximation of the

TCD
6, 2961–3010, 2012

force balance, horizontal variations in lateral vertical shearing are negligible in the vertical balance equation (Eq. A1). In other words, the ice overburden pressure is locally compensated meaning that any bridging effects supporting ice weight sideways are comparably small.

$$\partial_i(2\tau_{ii} + \tau_{jj}) + \partial_j\tau_{ij} + \partial_z\tau_{iz} = \rho g \partial_i s \qquad \text{for} \qquad i \neq j \tag{A7}$$

$$\dot{\varepsilon}_{iz} = \frac{1}{2}\partial_z u_i \tag{A8}$$

This variant of a higher-order model holds a second simplification that makes the force balance independent of vertical velocities and thus allows to solely solve for the horizontal components. This decoupling becomes possible by considering horizontal gradients in the vertical velocity field small compared to vertical gradients in the horizontal components $\partial_i v_z << \partial_z v_i$ (cf. Eq. A8). The vertical velocity component is in turn determined by mass conservation, i.e. incompressibility (Eq. A2).

A2 Basal resistance

The SIA and HO approaches are completed by three options to determine the basal resistance (see Table 2). In general the basal drag compensates effects from vertical plane shearing but modified by force transmission via the membrane stresses.

$$\tau_{bi}^{\parallel} = \tau_{iz}^{(b)} - \left(2\tau_{ii}^{(b)} + \tau_{jj}^{(b)}\right)\partial_i b - \tau_{ij}^{(b)}\partial_j b \qquad \text{for } i \neq j \quad \text{and } i,j \in \{x,y\} \tag{A9}$$

This equation describes the most general form of resistance at the ice bed interface. A first option for basal resistance arises from assumptions made for the SIA. Neglecting effects from membrane stresses, basal drag is balanced by vertical plane shearing at the base, which equals the driving stress τ_d.

$$\tau_{bi}^{\parallel} = \tau_{di} = -\rho g H \partial_i s \tag{A10}$$

TCD
6, 2961–3010, 2012

Calculating the basal drag in this way is referred to as the driving stress (DR) option. In contrast to this dominance of vertical plane shearing at the base is an approach that highlights the importance of membrane stresses. It stems from assuming a vertically uniform stress and velocity field, thus no vertical plane shearing, while the whole setup is balance by membrane stresses. In analogy to Bueler and Brown (2009) and using identical frictional forcing at the ice surface and its base, the resulting force balance is used to determine the basal stress field.

$$\tau_{\mathrm{b}i}^{\parallel} = -\rho g H \partial_i s - \partial_i \left(2H\tau_{ii}^{(\mathrm{b})\circ} + H\tau_{jj}^{(\mathrm{b})\circ}\right) - \partial_j \left(H\tau_{ij}^{(\mathrm{b})\circ}\right) \qquad \text{for} \qquad i \neq j \tag{A11}$$

$$\tau_{ij}^{\circ} = 2\eta^{\circ}\dot{\varepsilon}_{ij}^{\circ} \qquad \eta^{\circ} = \frac{1}{2}A(T^{\bullet})^{-\frac{1}{n}}\dot{\varepsilon}_e^{\circ\,-\frac{1-n}{n}} \qquad \dot{\varepsilon}_e^{\circ 2} = \frac{1}{2}\sum_{ij}\dot{\varepsilon}_{ij}\dot{\varepsilon}_{ij} \tag{A12}$$

This resistance option with dominant membrane stresses (ME) resembles a shallow shelf approximation (SSA) apart that for our purpose it serves to determine the condition for the frictional basal boundary. As a result from vertical integration the effective viscosity η° is purely determined by horizontal strains that control the evolution of a floating shelf. In analogy to the HO ice deformation, a last option arises from the negligence of horizontal gradients in the vertical velocity field for the strain rates. As a consequence a HO version of the general resistance equation (Eq. A9) is obtained. This way of balancing the basal drag uses a slightly simplified resistance (SR) equation and is referred to as SR option. Together with two option for ice deformation, this gives six versions of treating basal resistance and deformation in our model (see Table 2).

Appendix B

Boundary conditions

In order to find a unique solution for Eqs. (A1)–(A3), boundary conditions are required. At the ice-free points around the lateral boundary we set not only the ice thickness H

TCD
6, 2961–3010, 2012

to zero but also the velocity field. This Dirichlet boundary condition is widely used in ice sheet modelling although resulting margin gradients are in essence dictated by grid spacing. For the vertical boundaries, conditions become more elaborate.

B1 Free surface

The upper surface boundary condition is set up in a similar way as the one for the base (Eq. A9) except that it must be evaluated at the surface ($z = s$).

$$\tau_{si}^{\parallel} = \tau_{iz}^{(s)} - \left(2\tau_{ii}^{(s)} + \tau_{jj}^{(s)}\right)\partial_i s - \tau_{ij}^{(s)}\partial_j s \quad \text{for} \quad i \neq j \quad \text{and} \quad i,j \in \{x,y\} \tag{B1}$$

However since the contact with the atmosphere does not provide any resistance to the ice flow, its drag is zero imposing an internal balance of stresses at the ice surface.

$$\tau_{si}^{\parallel} = 0 \tag{B2}$$

Note that for the SIA this relation is automatically fulfilled since vertical shearing becomes zero at the upper boundary.

B2 Basal sliding

In order to close the system of equations, boundary values have to be prescribed for the basal drag in Eq. (A9). In other words, one has to find a relation for basal sliding dependent on basal characteristics which influence is elaborate and still controversial (see Fowler, 2010). A main distinction has to be made between a pure ice bedrock contact and a case where ice rest on a layer of till. In the first case, sliding is controlled by regelation, enhanced creep, effective water pressure, bedrock roughness and cavitation geometry (Fowler, 2010; Schoof, 2005, 2010). When ice overlays a till layer, finding an appropriate sliding relation becomes more elaborate since a reasonable rheology for till must be formulated. As a granular material with a yield stress, observations confirm that till is well described assuming a plastic rheology (e.g. Tulaczyk, 2000). However

TCD
6, 2961–3010, 2012

field measurements on Iceland (Boulton and Hindmarsh, 1987) indicate a non-linear viscous rheology with an exponent of three ($m = 3$). Such a nonlinear mechanism was found to be a prerequisite for realistic inland transmission of tidal forcing in Antarctic ice streams (Gudmundsson, 2011).

$$\tau_{bi} = C\, H^m u_b^{\frac{1-m}{m}} u_{bi} \Leftrightarrow u_{bi} = \frac{A_{sl}}{H} \tau_b^{m-1} \tau_{bi} \Leftrightarrow H\beta^2 u_{bi} = \tau_{bi}^m \tag{B3}$$

$$C^{-\frac{1}{m}} = A_{sl} = \beta^{-2} \qquad \text{with} \qquad i, j \in \{x, y\} \tag{B4}$$

These are three common and analogue notations for a nonlinear basal friction equation or a nonlinear sliding relation. C is the friction parameter, while β^2 is the friction coefficient and both are inversely related to the basal sliding coefficient A_{sl}. An enhancement of sliding towards the ice sheet margin is introduced by a weighting of the coefficients with the ice thickness. Equation (B3) together with Eq. (A9) allow to solve the partial differential Eqs. (A1–A3) uniquely. However for practical reasons a partially linearised sliding relation is introduced.

$$u_{bi} = \frac{A_{sl}}{H} \tau_d^{m-1} \tau_{bi} \tag{B5}$$

Here the nonlinearity of the sliding relation is accounted for by the driving stress τ_d which is fully prescribed by ice geometry. This leaves a linear relation between basal velocities u_b and basal drag τ_b with a highly geometry dependent proportionality factor. Our linear solver can directly handle such a linear sliding relation. In order to solve the full nonlinear Eq. (B3) an iterative method is chosen that consecutively updates τ_b until convergence is reached (for more details see analogue viscosity update described in Fürst et al., 2011).

Acknowledgements. This research received funding from the ice2sea programme from the European Union 7th Framework Programme grant number 226375, the Research Foundation – Flanders (FWO) project NEEM-B, and the Belgian Federal Science Policy Office within its Research Programme on Science for a Sustainable Development under contract SD/CS/06A (iCLIPS). This publication has the ice2sea contribution number 131.

TCD
6, 2961–3010, 2012

References

Amundson, J. M., Fahnestock, M., Truffer, M., Brown, J., Luthi, M. P., and Motyka, R. J.: Ice melange dynamics and implications for terminus stability, Jakobshavn Isbrae Greenland, J. Geophys. Res.-Earth, 115, F01005, doi:10.1029/2009JF001405, 2010.

Bamber, J. L., Layberry, R. L., and Gogineni, S. P.: A new ice thickness, bed dataset for the Greenland ice sheet 1; measurement, data reduction, and errors, J. Geophys. Res.-Atmos., 106, 33773–33780, doi:10.1029/2001JD900054, 2001.

Bartholomew, I., Nienow, P., Mair, D., Hubbard, A., King, M. A., and Sole, A.: Seasonal evolution of subglacial drainage and acceleration in a Greenland outlet glacier, Nat. Geosci., 3, 408–411, doi:10.1038/NGEO863, 2010.

Benn, D. I., Warren, C. R., and Mottram, R. H.: Calving processes and the dynamics of calving glaciers, Earth-Sci. Rev., 82, 143–179, doi:10.1016/j.earscirev.2007.02.002, 2007.

Bougamont, M., Price, S., Christoffersen, P., and Payne, A. J.: Dynamic patterns of ice stream flow in a 3-D higher-order ice sheet model with plastic bed and simplified hydrology, J. Geophys. Res., 116, F04018, doi:10.1029/2011JF002025, 2011.

Boulton, G. S. and Hindmarsh, R. C. A.: Sediment deformation beneath glaciers: rheology and geological consequences, J. Geophys. Res., 92, 9059–9082, doi:10.1029/JB092iB09p09059, 1987.

Briner, J. P., Bini, A. C., and Anderson, R. S.: Rapid early Holocene retreat of a Laurentide outlet glacier through an Arctic fjord, Nat. Geosci., 2, 496–499, doi:10.1038/ngeo556, 2009.

Buchardt, S. L. and Dahl-Jensen, D.: Estimating the basal melt rate at NorthGRIP using a Monte Carlo technique, Ann. Glaciol., 45, 137–142, doi:10.3189/172756407782282435, 2007.

Bueler, E. and Brown, J.: Shallow shelf approximation as a "sliding law" in a thermomechanically coupled ice sheet model, J. Geophys. Res., 114, F03008, doi:10.1029/2008JF001179, 2009.

Christoffersen, P., Mugford, R. I., Heywood, K. J., Joughin, I., Dowdeswell, J. A., Syvitski, J. P. M., Luckman, A., and Benham, T. J.: Warming of waters in an East Greenland fjord prior to glacier retreat: mechanisms and connection to large-scale atmospheric conditions, The Cryosphere, 5, 701–714, doi:10.5194/tc-5-701-2011, 2011.

Fowler, A. C.: Weertman, Lliboutry and the development of sliding theory, J. Glaciol., 56, 965–972, doi:10.3189/002214311796406112, 2010.

TCD
6, 2961–3010, 2012

Fürst, J. J., Rybak, O., Goelzer, H., De Smedt, B., de Groen, P., and Huybrechts, P.: Improved convergence and stability properties in a three-dimensional higher-order ice sheet model, Geosci. Model Dev., 4, 1133–1149, doi:10.5194/gmd-4-1133-2011, 2011.

Graversen, R. G., Drijfhout, S., Hazeleger, W., van de Wal, R., Bintanja, R., and Helsen, M.: Greenland's contribution to global sea-level rise by the end of the 21st century, Clim. Dynam., 37, 1427–1442, doi:10.1007/s00382-010-0918-8, 2011.

Gudmundsson, G. H.: Ice-stream response to ocean tides and the form of the basal sliding law, The Cryosphere, 5, 259–270, doi:10.5194/tc-5-259-2011, 2011.

Hindmarsch, R. C. A.: The role of membrane-like stresses in determining the stability and sensitivity of the Antarctic ice sheets: back pressure and grounding line motion, Philos. T. Roy. Soc. A., 364, 1733–1767, doi:10.1098/rsta.2006.1797, 2006.

Holland, D. M., Thomas, R. H., De Young, B., Ribergaard, M. H., and Lyberth, B.: Acceleration of Jakobshavn Isbrae triggered by warm subsurface ocean waters, Nat. Geosci., 1, 659–664, doi:10.1038/ngeo316, 2008.

Howat, I. M., Joughin, I., Fahnestock, M., Smith, B. E., and Scambos, T. A.: Synchronous retreat and acceleration of Southeast Greenland outlet glaciers 2000–06: ice dynamics and coupling to climate, J. Glaciol., 54, 646–660, doi:10.3189/002214308786570908, 2008.

Howat, I. M., Box, J. E., Ahn, Y., Herrington, A., and McFadden, E. M.: Seasonal variability in the dynamics of marine-terminating outlet glaciers in Greenland, J. Glaciol., 56, 601–613, doi:10.3189/002214310793146232, 2010.

Howat, I. M. and Eddy, A.: Multi-decadal retreat of Greenland's marine-terminating glaciers, J. Glaciol., 57, 389–396, doi:10.3189/002214311796905631, 2011.

Hutter, K.: Theoretical Glaciology; Material Science of Ice and the Mechanics of Glaciers and Ice Sheets, D. Reidel Publishing Company/Tokyo, Terra Scientific Publishing Company, Dordrecht, Boston, Tokyo, Japan, and Hingham, MA, ISBN 9027714738, 1983.

Huybrechts, P.: The present evolution of the Greenland ice sheet – an assessment by modelling, Global Planet. Change, 9, 39–51, doi:10.1016/0921-8181(94)90006-X, 1994.

Huybrechts, P.: Sea-level changes at the LGM from ice-dynamic reconstructions of the Greenland and Antarctic ice sheets during the glacial cycles, Quat. Sci. Rev., 21, 203–231, doi:10.1016/S0277-3791(01)00082-8, 2002.

Huybrechts, P. and de Wolde, J.: The dynamic response of the Greenland and Antarctic ice sheets to multiple-century climatic warming, J. Climate, 12, 2169–2188, doi:10.1175/1520-0442(1999)012<2169:TDROTG>2.0.CO, 1999.

TCD
6, 2961–3010, 2012

Huybrechts, P., Goelzer, H., Janssens, I., Driesschaert, E., Fichefet, T., Goosse, H., and Loutre, M.-F.: Response of the Greenland and Antarctic ice sheets to multi-millennial greenhouse warming in the Earth system model of intermediate complexity LOVECLIM, Surv. Geophys., 32, 397–416, doi:10.1007/s10712-011-9131-5, 2011.

Joughin, I., Howat, I. M., Fahnestock, M., Smith, B., Krabill, W., Alley, R. B., Stern, H., and Truffer, M.: Continued evolution of Jakobshavn Isbrae following its rapid speedup, J. Geophys. Res., 113, F04006, doi:10.1029/2008JF001023, 2008.

Joughin, I., Smith, B. E., Howat, I. M., Scambos, T., and Moon, T.: Greenland flow variability from ice-sheet-wide velocity mapping, J. Glaciol., 56, 415–430, doi:10.3189/002214310792447734, 2010.

Jouvet, G., Huss, M., Blatter, H., Picasso, M., and Rappaz, J.: Numerical simulation of Rhonegletscher from 1824 to 2100, J. Comput. Phys., 228, 6426–6439, doi:10.1016/j.jcp.2009.05.033, 2009.

Kamb, B. and Echelmeyer, K. A.: Stress-gradient coupling glacier flow, 1. longitudinal averaging of the influence of ice thickness and surface slope, J. Glaciol., 32, 267–284, 1986.

Lliboutry, L.: General theory of subglacial cavitation and sliding of temperate glaciers, J. Glaciol., 7, 21–58, 1968.

Luthcke, S. B., Zwally, H. J., Abdalati, W., Rowlands, D. D., Ray, R. D., Nerem, R. S., Lemoine, F. G., McCarthy, J. J., and Chinn, D. S.: Recent Greenland ice mass loss by drainage system from satellite gravity observations, Science, 314, 1286–1289, doi:10.3189/002214308784886117, 2006.

McFadden, E. M., Howat, I. M., Joughin, I., Smith, B., and Ahn, Y.: Changes in the dynamics of marine terminating outlet glaciers in West Greenland (2000–2009), J. Geophys. Res., 116, F02022, doi:10.1029/2010JF001757, 2011.

Moon, T., Joughin, I., Smith, B., and Howat, I.: 21st century evolution of Greenland outlet glacier velocities, Science, 336, 576–578, doi:10.1126/science.1219985, 2012.

Motyka, R. J., Truffer, M., Fahnestock, M., Mortensen, J., Rysgaard, S., and Howat, I.: Submarine melting of the 1985 Jakobshavn Isbrae floating tongue and the triggering of the current retreat, J. Geophys. Res., 116, F01007, doi:10.1029/2009JF001632, 2011.

Nick, F. M., Vieli, A., Howat, I. M., and Joughin, I.: Large-scale changes in Greenland outlet glacier dynamics triggered at the terminus, Nat. Geosci., 2, 110–114, doi:10.1038/NGEO394, 2009.

TCD
6, 2961–3010, 2012

Nick, F. M., van der Veen, C. J., Vieli, A., and Benn, D. I.: A physically based calving model applied to marine outlet glaciers and implications for the glacier dynamics, J. Glaciol., 56, 781–794, doi:10.3189/002214310794457344, 2010.
Pattyn, F.: A new three-dimensional higher-order thermomechanical ice sheet model: basic sensitivity, ice stream development, and ice flow across subglacial lakes, J. Geophys. Res.-Sol. Ea., 108, doi:10.1029/2002JB002329, 1–15, 2003.
Phillips, T., Rajaram, H., and Steffen, K.: Cryo-hydrologic warming: a potential mechanism for rapid thermal response of ice sheets, Geophys. Res. Lett., 37, L20503, doi:10.1029/2010GL044397, 2010.
Price, S. F., Payne, A. J., Catania, G. A., and Neumann, T. A.: Seasonal acceleration of inland ice via longitudinal coupling to marginal ice, J. Glaciol., 54, 213–219, 2008.
Price, S. F., Payne, A. J., Howat, I. M., and Smith, B.: Committed sea-level rise for the next century from Greenland ice sheet dynamics during the past decade, Proc. Natl. Acad. Sci., 108, 8978–8983, doi:10.1073/pnas.1017313108, 2011.
Raymond, C. F.: Deformation in the vicinity of ice divides, J. Glaciol., 29, 357–373, 1983.
Rignot, E. and Kanagaratnam, P.: Changes in the velocity structure of the Greenland ice sheet, Science, 311, 986–990, doi:10.1126/science.1121381, 2006.
Rignot, E., Velicogna, I. van den Broeke, M. R., Monaghan, A., and lenaerts, J.: Acceleration of the contribution of the Greenland and Antarctic ice sheets to sea level rise, Geophys. Res. Lett., 38, L05503, doi:10.1029/2011GL046583, 2011.
Ritz, C., Rommelaere, V., and Dumas, C.: Modeling the evolution of Antarctic ice sheet over the last 420,000 years: implications for altitude changes in the Vostok region, J. Geophys. Res.-Atmos., 106, 31943–31964, doi:10.1029/2001JD900232, 2001.
Scambos, T. A., Hulbe, C., Fahnestock, M., and Bohlander, J.: The link between climate warming and break-up of ice shelves in the Antarctic Peninsula, J. Glaciol., 46, 516–530, 2000.
Schoof, C.: The effect of cavitation on glacier sliding, Proc. R. Soc. Lond. Ser. A, 461, 609–627, doi:10.1098/rspa.2004.1350, 2005.
Schoof, C.: A variational approach to ice streams flow, J. Fluid. Mech., 556, 227–251, doi:10.1017/S0022112006009591, 2006.
Schoof, C.: Ice sheet grounding line dynamics: steady states, stability, and hysteresis, J. Geophys. Res., 112, F03S28, doi:10.1029/2006JF000664, 2007.
Schoof, C.: Ice-sheet acceleration driven by melt supply variability, Nature, 468, 803–806, doi:10.1038/nature09618, 2010.

TCD
6, 2961–3010, 2012

Schoof, C. and Hindmarsh, R. C. A.: Thin-film flows with wall slip: an asymptotic analysis of higher order glacier flow models, Q. J. Mech. Appl. Math., 63, 73–114, doi:10.1093/qjmam/hbp025, 2009.
Schrama, E. J. O. and Wouters, B.: Revisiting Greenland ice sheet mass loss observed by GRACE, J. Geophys. Res., 116, B02407, doi:10.1029/2009JB006847, 2011.
Seddik, H., Greve, R., Zwinger, R., Gillet-Chaulet, F., and Gagliardini, O.: Simulations of the Greenland ice sheet 100 years into the future with the full Stokes model Elmer/Ice, J. Glaciol., 58, 448–456, doi:10.3189/2012JoG11J177, 2012.
Slobbe, D. C., Lindenbergh, R. C., and Ditmar, P.: Estimation of volume change rates of Greenland's ice sheet from ICESat data using overlapping footprints, Remote Sens. Environ., 112, 4204–4213, doi:10.1016/j.rse.2008.07.004, 2008.
Sørensen, L. S., Simonsen, S. B., Nielsen, K., Lucas-Picher, P., Spada, G., Adalgeirsdottir, G., Forsberg, R., and Hvidberg, C. S.: Mass balance of the Greenland ice sheet (2003–2008) from ICESat data – the impact of interpolation, sampling and firn density, The Cryosphere, 5, 173–186, doi:10.5194/tc-5-173-2011, 2011.
Straneo, F., Hamilton, G. S., Sutherland, D. A., Stearns, L. A., Davidson, F., Hammill, M. O., Stenson, G. B., and Rosing-Asvid, A.: Rapid circulation of warm subtropical waters in a major glacial fjord in East Greenland, Nat. Geosci., 3, 182–186, doi:10.1038/NGEO764, 2010.
Straneo, F., Curry, R. G., Sutherland, D. A., Hamilton, G. S., Cenedese, C., Vage, K., and Stearns, L. A.: Impact of fjord dynamics and glacial runoff on the circulation near Helheim Glacier, Nat. Geosci., 4, 322–327, doi:10.1038/NGEO1109, 2011.
Sundal, A. V., Sheperd, A., Nienow, P., Hanna, E., Palmer, S., and Huybrechts, P.: Melt-induced speed-up of Greenland ice sheet offset by efficient subglacial drainage, Nature, 469, 521–524, doi:10.1038/nature09740, 2011.
Thomas, R., Frederick, E., Krabill, W., Manizade, S., and Martin, C.: Recent changes on Greenland outlet glaciers, J. Glaciol., 55, 147–162, doi:10.3189/002214309788608958, 2009.
Tulaczyk, S., Kamb, W. B., and Engelhardt, H. F.: Basal mechanics of Ice Stream B, West Antarctica, 1. till mechanics, J. Geophys. Res.-Sol. Ea., 105, 463–481, doi:10.1029/1999JB900329, 2000.
van den Broeke, M. R., Bamber, J., Ettema, J., Rignot, E., Schrama, E., van de Berg, W.-J., van Meijgaard, E., Velicogna, I., and Wouters, B.: Partitioning recent Greenland mass loss, Science, 326, 984–986, doi:10.1126/science.1178176, 2009.

TCD
6, 2961–3010, 2012

Velicogna, I.: Increasing rates of ice mass loss from the Greenland and Antarctic ice sheets revealed by GRACE, Geophys. Res. Lett., 36, L19503, doi:10.1029/2009GL040222, 2009.
Weertman, J.: Deformation of floating ice shelves, J. Glaciol., 3, 38–42, 1957.
Weertman, J.: The theory of glacier sliding, J. Glaciol., 5, 287–303, 1964.
Williams, C. R., Hindmarsh, R. C. A., and Arthern, R. J.: Frequency response of ice streams, Proc. R. Soc. A, published online, doi:10.1098/rspa.2012.018, 2012.
Zwally, H. J., Abdalati, W., Herring, T., Larson, K., Saba, J., and Steffen, K.: Surface melt-induced acceleration of Greenland ice-sheet flow, Science, 297, 218–222, doi:10.1126/science.1072708, 2002.
Zwally, H. J., Giovinetto, M. B., Li, J., Cornejo, H. G., Beckley, M. A., Brenner, A. C., Saba, J. L., and Yi, D. H.: Mass changes of the Greenland and Antarctic ice sheets and shelves and contributions to sea-level rise: 1992–2002, J. Glaciol., 51, 509–527, doi:10.3189/172756505781829007, 2005.
Zwally, H. J., Li, J., Brenner, A. C., Beckley, M., Cornejo, H. G., Dimarzio, J., Giovinetto, M. B., Neumann, T. A., Robbins, J., Saba, J., Yi, D. H., Wang, W. L.: Greenland ice sheet mass balance: distribution of increased mass loss with climate warming; 2003–07 versus 1992–2002, J. Glaciol., 57, 88–102, doi:10.3189/002214311795306682, 2011.
Zwinger, T., Greve, R., Gagliardini, O., Takayuki, S., and Lyly, M.: A full Stokes-flow thermo-mechanical model for firn and ice applied to the Gorshkov crater glacier, Kamchatka, Ann. Glaciol., 45, 29–37, doi:10.3189/172756407782282543, 2007.

TCD
6, 2961–3010, 2012

Table 1. Parameter overview.

Symbol	Description		Value	Unit
Physical properties				
g	Gravitational acceleration constant		9.81	$\mathrm{m\,s^{-2}}$
ρ	Average density of ice body		910	$\mathrm{kg\,m^{-3}}$
R	Universal gas constant		8.314	$\mathrm{J\,mol^{-1}\,K^{-1}}$
Ice deformation				
A_1	Coefficients in Arrhenius equation for	$T^\bullet < T_c$	3.99×10^{-5}	$\mathrm{Pa^{-3}\,yr^{-1}}$
A_2		$T^\bullet > T_c$	1.91×10^{10}	
B_1	Factors in Arrhenius equation for	$T^\bullet < T_c$	50×10^3	$\mathrm{J\,mol^{-1}}$
B_2		$T^\bullet > T_c$	139×10^3	
n	Exponent in Glen's flow equation		3	–
T_c	Temperature threshold for enhanced ice creep		263.15	K
Basal sliding				
A_{sl}	Sliding coefficient		10^{-10}	$\mathrm{Pa^{-3}\,m^2\,yr^{-1}}$
C	Friction coefficient		2154.421	$\mathrm{Pa\,m^{-6}\,yr}$
m	Exponent in Budd/Wertman type sliding law		3	–

TCD
6, 2961–3010, 2012

Table 2. Overview of model versions with different approaches to describe ice deformation and basal resistance. Note that the combination ME HO is omitted in this work since SR HO provides both a more comprehensive and natural setup. For details of each approach refer to Appendix B.

		Ice Deformation	
		Shallow Ice Approximation	Higher-order Approach
Basal Resistance	Driving Stress	DR SIA	DR HO
	Membrane Stresses	ME SIA	ME HO
	Simplified Resistance	SR SIA	SR HO

TCD
6, 2961–3010, 2012

Table 3. Overview of the presented experiments.

Abbreviation	Experiment Description
MarAsl2	Doubling the sliding factor upstream of marine terminated outlets.
TotAsl2	Doubling the sliding factor over the entire sliding area.
MarCut	Singular calving event for marine terminus reaching 40 km inland.

TCD
6, 2961–3010, 2012

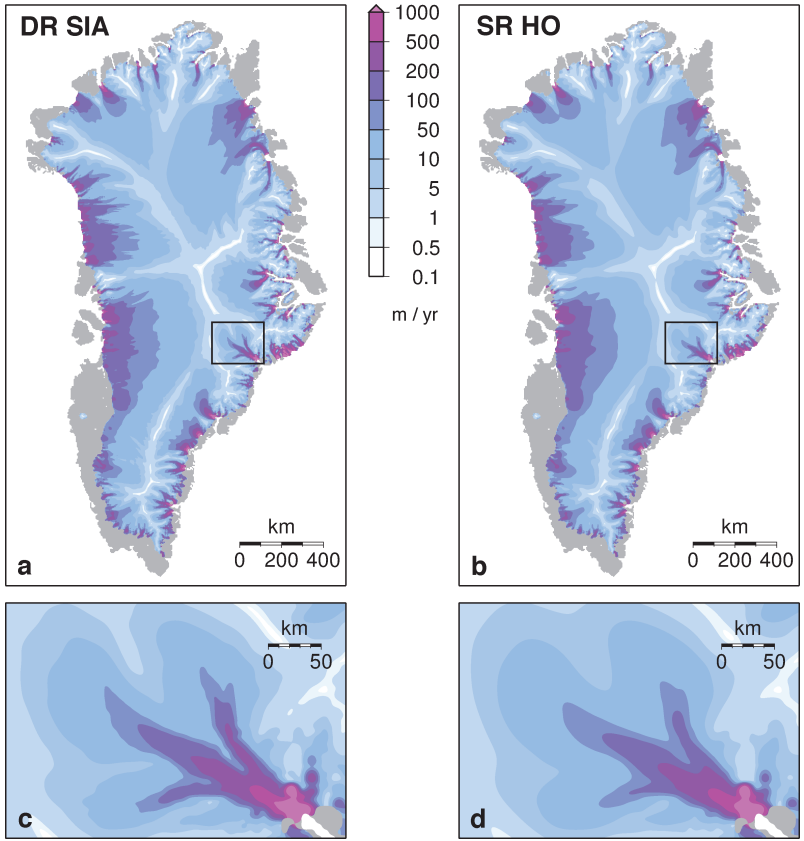

Fig. 1. Surface velocity magnitude for the IS standard interglacial equilibrium with continental outline in grey. The underlying geometry is obtained with the DR SIA model. **(a, c)** show the velocity magnitude for DR SIA while their higher-order equivalent from SR HO is presented in **(b, d)** for the same geometry. The lower two panels **(c, d)** show a close-up around Kangerlugssuaq.

TCD
6, 2961–3010, 2012

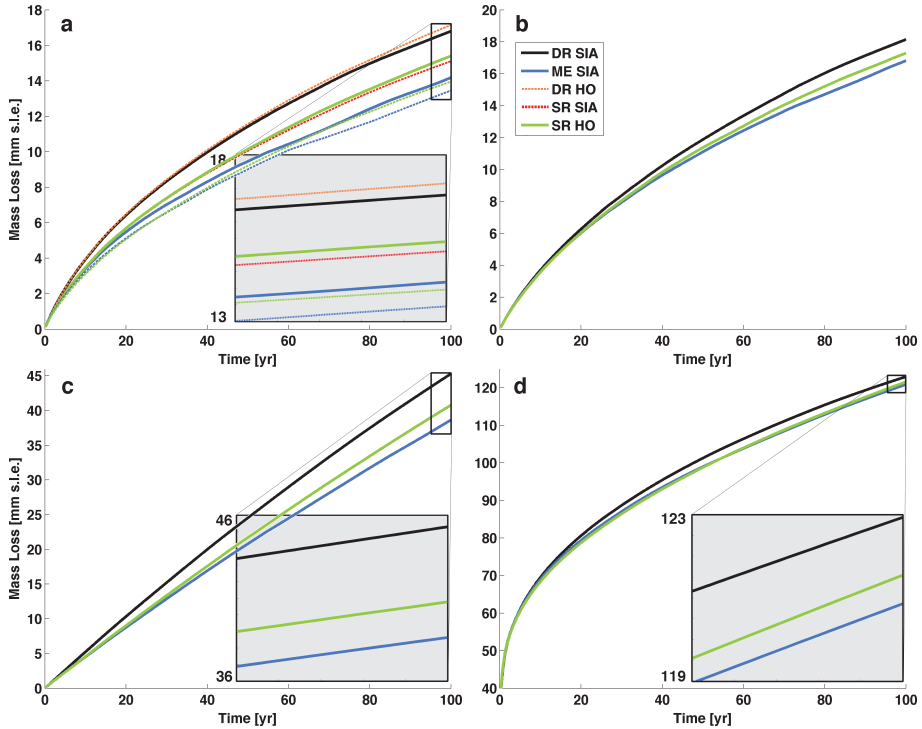

Fig. 2. Ice mass loss of different model versions on 5 km resolution for the three forcing scenarios: **(a)** MarAsl2, **(c)** TotAsl2, **(d)** MarCut started from IS while in **(b)** MarAsl2 is initiated from PS. Mass loss is determined by subtracting any background signal of a control experiment from the forcing experiment. Mass loss differs not more than 20 % amongst the model versions and results are robust under different initial conditions **(a, b)**. Each close-up zooms in on the last 5 yr of the experiments. The dashed blue (ME SIA) and green (SR HO) line represent the respective model version using a full non-linear sliding law (see Appendix B).

TCD
6, 2961–3010, 2012

Effect of higher-order stress gradients

J. J. Fürst et al.

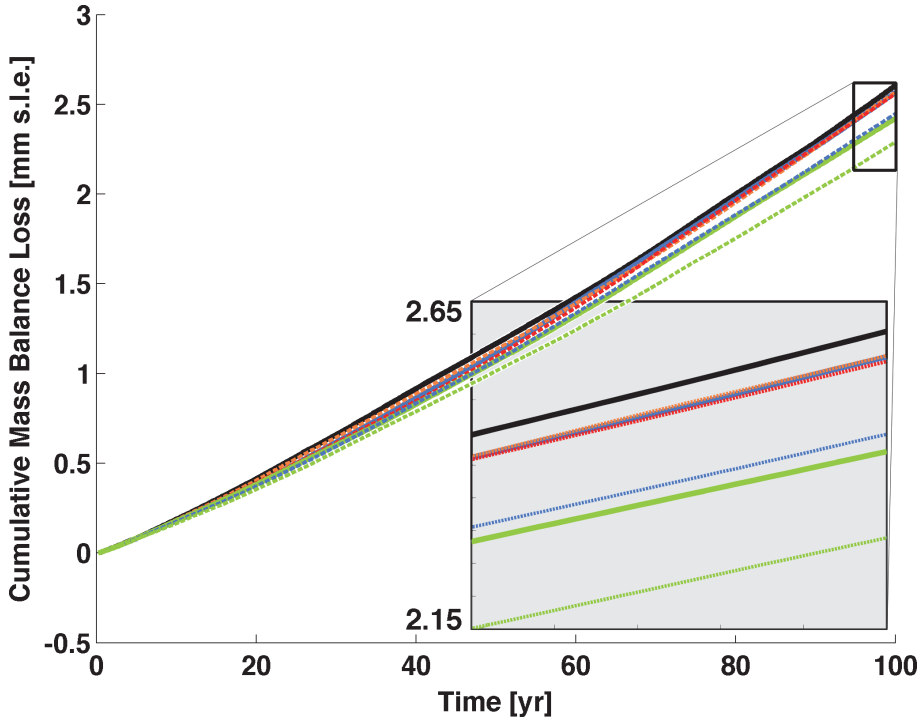

Fig. 3. Transient evolution of cumulative surface mass balance for the MarAsl2 experiment initiated from IS with respect to a control run. The surface mass balance increases almost linearly and higher-order dynamics mainly alter the final magnitude. Inconsistencies in the feedback sign and magnitude on the various resolutions exclude it from being the crucial process for differences in the centennial mass loss.

TCD
6, 2961–3010, 2012

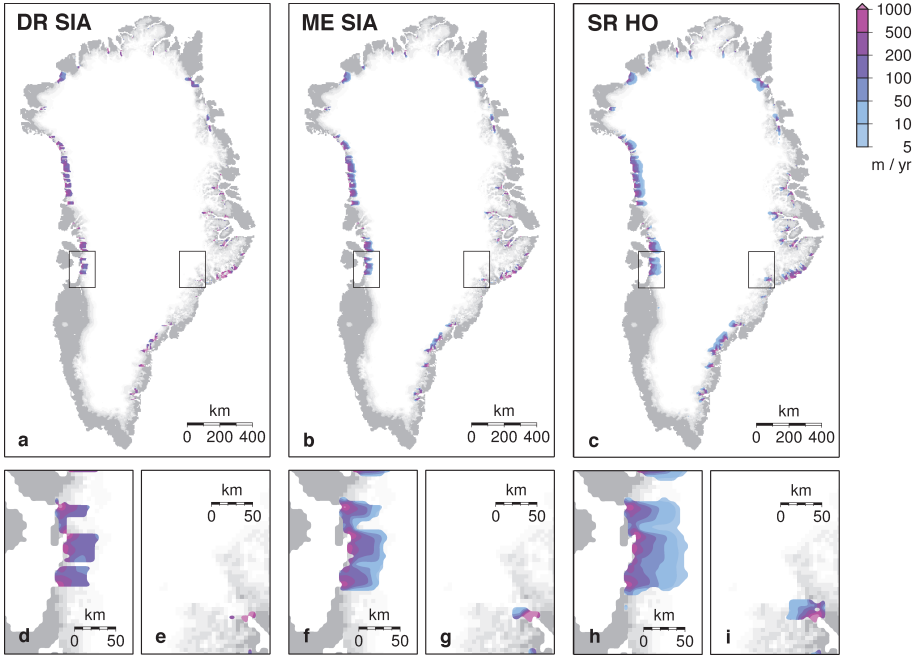

Fig. 4. Initial response in surface velocities to the MarAsl2 perturbation for the three main model versions. Initiated from the 5 km IS, the geometry is still identical although the A_{sl} forcing already operates. Shown are accelerations with respect to a control experiment run for each model version. In the DR SIA setup **(a)**, the marginal accelerations are inherently confined to the forcing area. The close-ups of Jakobshavn Isbræ **(d)** and Kangerlugssuaq **(e)** allow to clearly identify the grid cells that experience A_{sl} amplification. In the ME SIA **(b, f, g)** and SR HO setup **(c, h, i)**, direct horizontal coupling is included and effects from both longitudinal stresses and transverse horizontal shearing are distinguishable.

TCD
6, 2961–3010, 2012

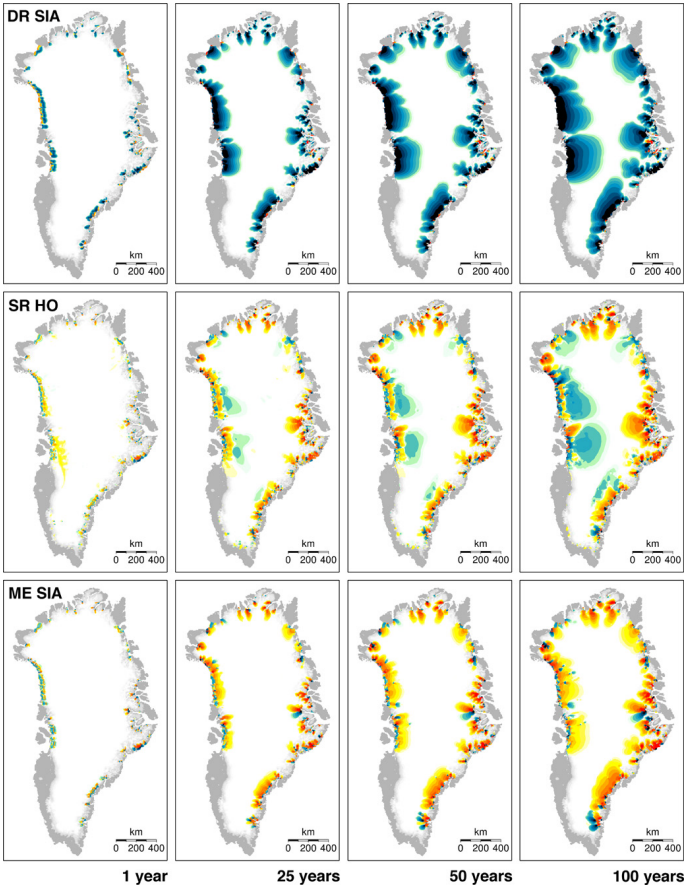

Fig. 5. (Caption on next page.)

TCD
6, 2961–3010, 2012

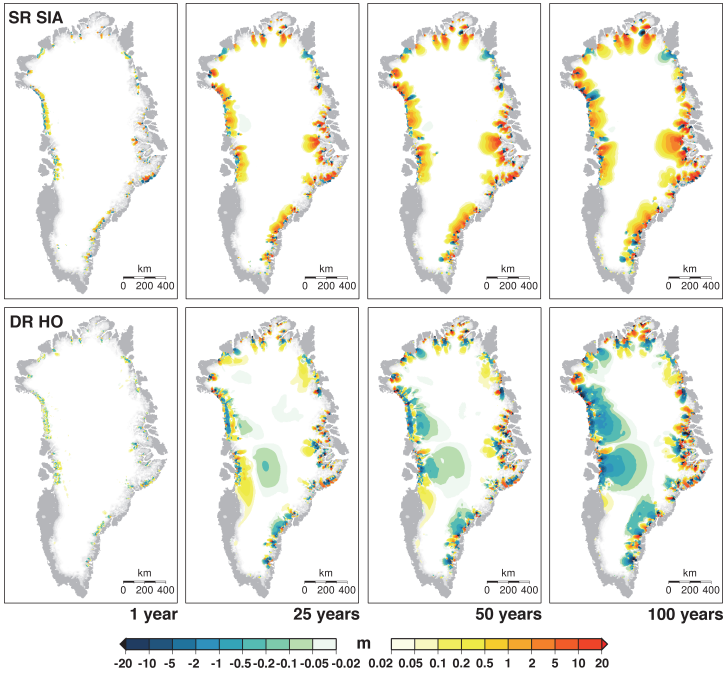

Fig. 5. Ice thickness evolution for the 5 km MarAsl2 experiment for all five model versions started from the IS state. The upper panels show the DR SIA ice thickness differences with respect to its control run after respectively 1, 25, 50 and 100 yr. Ice thickness changes in the other model versions are shown with respect to the dominant DR SIA differences.

TCD
6, 2961–3010, 2012

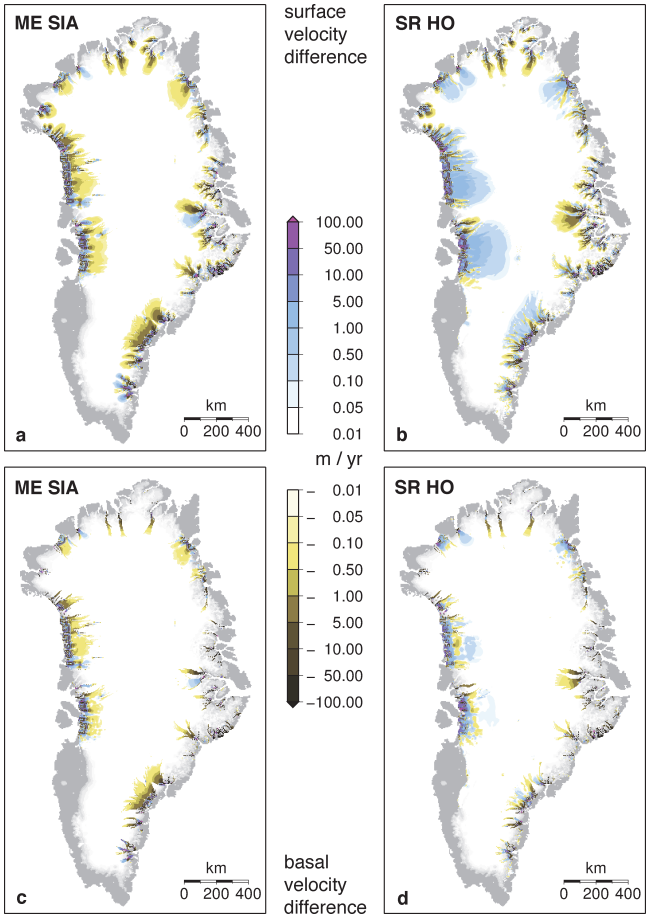

Fig. 6. Ice velocity evolution for the 5 km MarAsl2 experiment after 50 yr for ME SIA **(a, c)** and SR HO **(b, d)** starting from IS. Surface velocities (upper panels) and basal velocities (lower panels) are shown as absolute differences to the DR SIA evolution.

TCD
6, 2961–3010, 2012

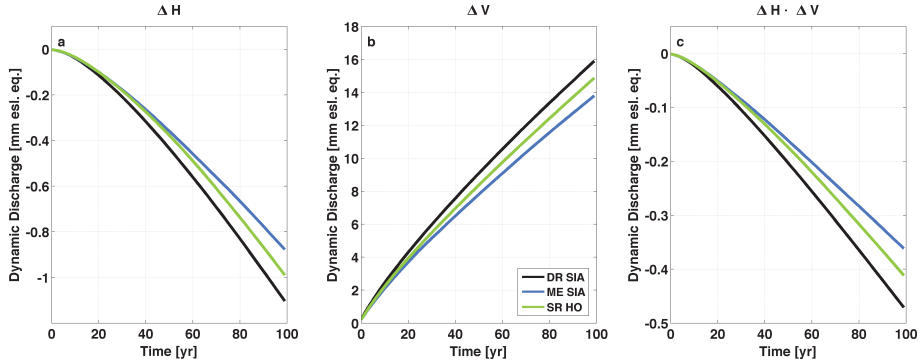

Fig. 7. Decomposition of the dynamics discharge signal of MarAsl2 into contributions from different evolution in **(a)** ice thickness alone, **(b)** velocity magnitudes alone and **(c)** and their combination (cf. Eq. 1). Note that only together with melt water runoff from the ice sheet all these curves add up to the total volume loss in Fig. 2a.

TCD
6, 2961–3010, 2012

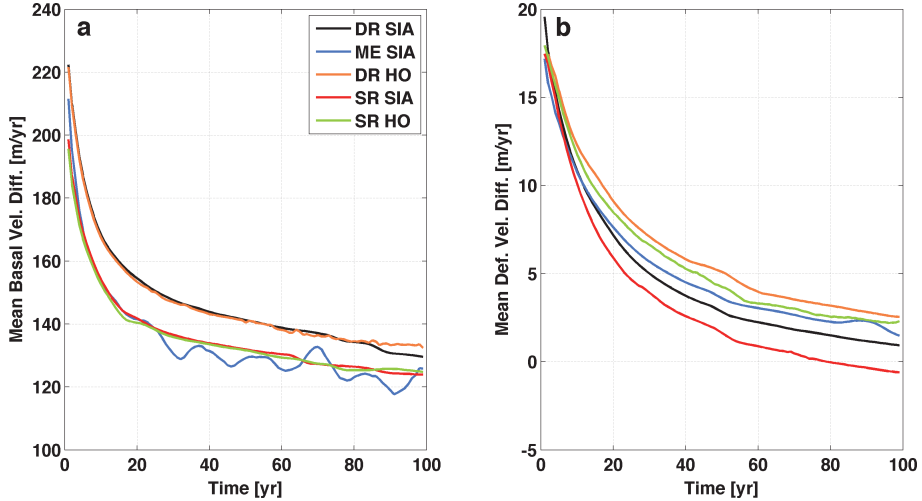

Fig. 8. Spatially averaged velocity response in MarAsl2 for the marginal sliding region decomposed into its basal **(a)** and mean deformational component **(b)**. Background velocities from an unforced control experiment are subtracted. Due to changes in the extent of the sliding area both average values were linearly smoothed.

TCD
6, 2961–3010, 2012

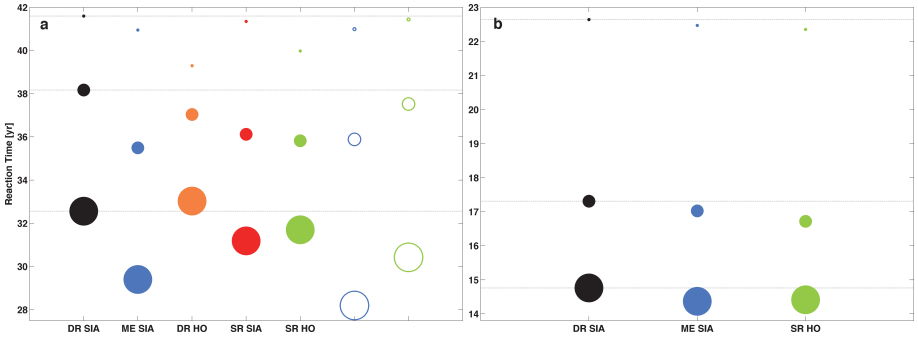

Fig. 9. Mean reaction time retrieved for each experiment: **(a)** MarAsl2 and **(b)** MarCut. The dot sizes indicate the resolution on which the experiment was conducted. The largest and smallest dot size represents respectively the 5 and 20 km grid. Response time is calculated from Eq. (3) and averaged for comparison. This time scale reflects the immediate response to a stepwise perturbation rather than a full ice sheet equilibration of many thousand years.

TCD
6, 2961–3010, 2012